# Localization of helical edge states in the absence of external magnetic field

A. V. Bubis,[1,2] N. N. Mikhailov,[3,4] S. A. Dvoretsky,[3] A. G. Nasibulin,[1,5] and E. S. Tikhonov[2,6,*]

[1]*Skolkovo Institute of Science and Technology, Nobel Street 3, Moscow 143026, Russian Federation*
[2]*Institute of Solid State Physics, Russian Academy of Sciences, Chernogolovka 142432, Russian Federation*
[3]*Institute of Semiconductor Physics, Novosibirsk 630090, Russian Federation*
[4]*Novosibirsk State University, Novosibirsk 630090, Russian Federation*
[5]*Aalto University, P.O. Box 16100, 00076 Aalto, Finland*
[6]*National Research University Higher School of Economics, 20 Myasnitskaya Street, Moscow 101000, Russian Federation*

(Received 26 April 2021; revised 23 June 2021; accepted 25 October 2021; published 5 November 2021)

Theoretically, the helical edge states of two-dimensional topological insulators are protected from coherent backscattering due to nonmagnetic disorder provided electron interactions are not too strong. Experimentally, the edges typically do not demonstrate systematic and robust quantization, but at the same time little is known about the sub-Kelvin temperature behavior. Here, we report the surprising localization of the edge states in an 8-nm HgTe quantum well in zero magnetic field at millikelvin temperatures. Additionally, the magnetoresistance data at 0.5 K for edges a few micrometers long suggest the field-dependent localization length $l_B \propto B^{-\alpha}$, with $\alpha$ ranging approximately from 1.6 to 2.8 at fields $B \lesssim 0.1$ T and $\alpha \approx 1.1$ at higher fields up to 0.5 T. In the frame of the disordered interacting edge, these values of $\alpha$ correspond to the Luttinger liquid parameters $K \approx 0.9$–$1.1$ and $K \approx 0.6$, respectively. We discuss possible scenarios which could result in zero magnetic field localization.

DOI: 10.1103/PhysRevB.104.195405

## I. INTRODUCTION

The concept of the quantum spin Hall (QSH) effect [1,2] is manifested in the existence of gapped bulk insulators with the edge conduction due to helical electrons for which the spin and the momentum are locked. Time-reversal symmetry (TRS) protects edge channels of these two-dimensional topological insulators (2D TIs) against single-particle coherent backscattering. From here, in the experiment at low enough temperature $T$ one could have naively expected the quantized edge conductance $G_q = e^2/h$. Still, it is common that at low $T$ one usually observes almost absent or only very weak $T$ dependence for the edge conductances $G \ll G_q$ [3]. Such behavior is believed to be due to as yet unexplained phase-breaking mechanisms but may be phenomenologically captured, e.g., in the model of the conducting charge puddles in the insulating bulk of a 2D TI [4].

Beyond the single-particle description, it was realized early on that the picture of ideal helical edge states can be significantly modified by two-particle scattering processes [5,6]. The strength of the omnipresent interelectron Coulomb interaction is usually expressed in terms of the Luttinger liquid parameter $K$ which is also dependent on the Fermi velocity $v_F$ and the system geometry [7,8]. The value of $K$, with $0 < K < 1$ corresponding to repulsive interactions and $K = 1$ corresponding to the noninteracting electrons, crucially defines the transport properties of a 2D TI [9]. As an example, a recent theoretical paper [10] studied the phase diagram of a disordered interacting edge and predicted the possibility of an insulating edge for strong enough interactions $K < 3/8$. This is in line with early works [5,6] predicting the possibility of localization for strong enough interactions.

So far, only a few experimental studies have addressed the measurements of $K$ in the helical edge channels [11,12]. The interpretation of the temperature dependence of the conductance or the bias dependence of the differential conductance in a transport experiment may be ambiguous since the extracted value of $K$ depends on the underlying theory [11,13]. This approach is further complicated by the fact that above 1 K, $R(T)$ behavior is usually weak [3] while the data at sub-Kelvin temperatures are scarce and poorly consistent with each other [14–18]. At the same time, the tunneling spectroscopy approach of Ref. [12] is not applicable to the most studied HgTe/CdTe and InAs/GaSb realizations of 2D TIs. We also mention that the proposed corner junction experiments on the interedge tunneling [19,20] have not yet been realized, the notable recent exception being the experiment in the standard quantum point contact geometry [21]. There, the edge channels from opposite sides of a device were guided into a quasi-one-dimensional constriction and an additional conductance plateau at $G_q$ was observed, indicating the interaction-driven opening of a spin gap. Concerning the experimental determination of $K$ [11,12], we note that the situation may be additionally complicated by the possible presence of magnetic impurities [22], Rashba spin-orbit coupling originating from the electric field of the gate electrode [23], or a hyperfine interaction with the nuclear spins [24].

Since TRS is an essential ingredient for topological protection, an external magnetic field is an important knob to provide additional information. The introduction of a

*tikhonov@issp.ac.ru

 

magnetic field opens a Zeeman gap in the edge spectrum [25] and couples the counterpropagating edge modes. As a result, the restored coherent backscattering must decrease the conductance or even localize the edges, provided the phase coherence is preserved. This common anticipation, while partly confirmed already in the very first experimental paper [26], was later on contrasted with the observations of only weakly $B$-dependent transport in both InAs/GaSb and HgTe quantum wells (QWs) [15,27]. Theoretically, this robustness of the edge-state transport to magnetic fields as high as several tesla was later attributed to the Dirac point being hidden in the bulk band rather than in the bulk gap [28,29]. On the other hand, localization was recently reported for the helical edges in $d = 8$ and 14 nm HgTe QWs with drastic changes in conductance for the $d = 8$ nm case already at a few mT perpendicular fields [18]. With similar behavior of both quasiballistic and resistive edges in a zero $B$ field down to the lowest temperatures, this experiment demonstrated that the edge transport with $G \ll G_q$ is in fact due to topological protection. Similarly, further studies of the interacting edges in InAs/GaSb QWs also demonstrated the possibility of strong resistance growth at increasing $B$ with only weak $T$ dependence in zero magnetic field [30]. Overall, one has to admit no clear picture of the magnetic-field-dependent localization of the helical edge states exists at the moment.

## II. DEVICES AND MEASUREMENT TECHNIQUE

In the present paper, we demonstrate that helical edges may localize at millikelvin temperatures even in zero magnetic field and discuss the possible scenarios of localization. Our samples are based on the 8-nm-wide HgTe/CdHgTe QW grown by molecular beam epitaxy on a (013) GaAs substrate [31] (see Fig. 1). For patterning of the mesa we used e-beam lithography followed by wet mesa etching in an aqueous solution of KI:$I_2$:HBr. This approach [32] resulted in an uncontaminated mesa sidewall, thus the thin HgTe layer could be observed by scanning electron microscopy (SEM) [see the narrow white line in Fig. 1(b)]. Further, Ti/Al contacts were evaporated right after *in situ* cap removal with the Ar gun. The 70-nm $SiO_2$ gate dielectric is then magnetron sputtered followed by Ti/Al gate electrode deposition. During fabrication the heating of the substrate was carefully controlled with the highest temperature of 80 °C utilized for resist baking. Below we present the data from two geometrically similar devices D1 and D2 etched simultaneously. Due to technical difficulties, we were not able to cool down device D1 to millikelvin temperatures. The measurements at 4.2 and 0.5 K were performed in a $^3$He insert with the external magnetic field perpendicular to the QW plane. The measurements at lower temperatures were performed in a BlueFors-LD250 dilution refrigerator not equipped with a solenoid. From the Johnson-Nyquist noise thermometry we estimate the lowest achievable electron temperature as 70 mK. The $I$-$V_{sd}$ curves were measured using either a homemade transimpedance amplifier (feedback resistance $Z_{fb} = 100$ MΩ) or homemade voltage preamplifier (input impedance $Z_{input} = 10$ GΩ). The details of DC line filtering may be found in the Supplemental Material [33].

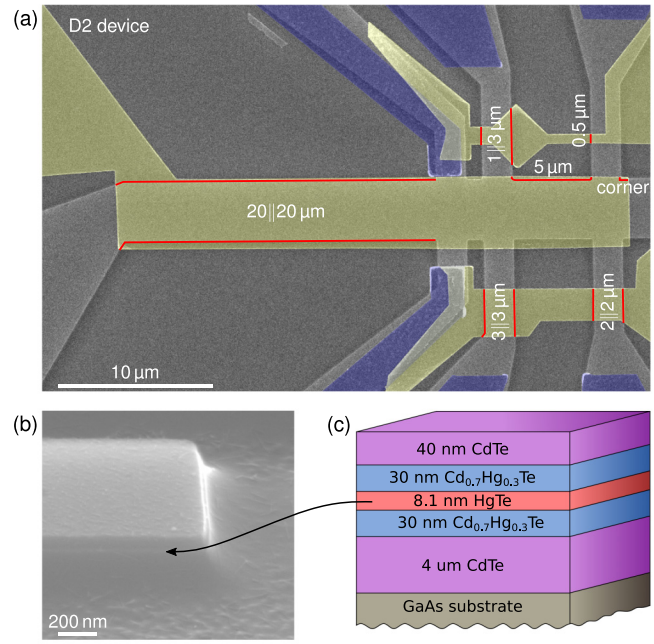


FIG. 1. (a) False color SEM micrograph of the device D2. Three galvanically isolated top gate electrodes are marked with yellow. The evaporated aluminum contacts are colored in blue. Studied edges are indicated by red lines captioned the same way they are mentioned in the text. (b) The mesa after wet etching. The 8-nm-wide QW is visible as a narrow white line. (c) Schematic view of the heterostructure before the lithography. The helical edge states exist along the boundary of the HgTe layer (red).

## III. EXPERIMENTAL RESULTS AND DISCUSSION

In our devices, the QSH regime is realized by tuning the Fermi energy level to the bulk energy gap using the voltage $V_g$ applied to the gate electrode. At low temperatures, the devices demonstrate typical dependencies of resistance on the gate voltage $V_g$. For the case of the 20-$\mu$m edge [see Fig. 2(a)], gate voltages $V_g > -3.4$ V correspond to the $n$-type conduction in the bulk, gate voltages $V_g < -4.5$ V correspond to the $p$-type conduction in the bulk, while the intermediate range of $V_g$ corresponds to the case when the Fermi level is inside the insulating bulk. In this region of $V_g$, the so-called charge neutrality point region (CNP), the conduction through the device is dominated by the edge states, which is manifested as a maximum in the dependence $R(V_g)$. Note that the exact range of gate voltages corresponding to the CNP may differ for different devices. In the CNP, the $I$-$V_{sd}$ curves are close to linear [see the inset of Fig. 2(a)]. We note that for the edges not longer than a few micrometers we generally do not see any systematic dependence of resistance $R$ on the edge length $L$ with the values of resistance at the CNP on the order of 100 kΩ at 4.2 K. For the longer edges the dependencies $R(L)$ are monotonously growing.

We verify the edge transport at the CNP using the voltage measurements on the contacts seemingly not lying on the current path [17,34–36] (see Supplemental Material Fig. S1 [33]). At the CNP, the voltage along the edge of the device monotonously falls when moving from the biased contact to the ground reflecting the negligible bulk transport. One can es-

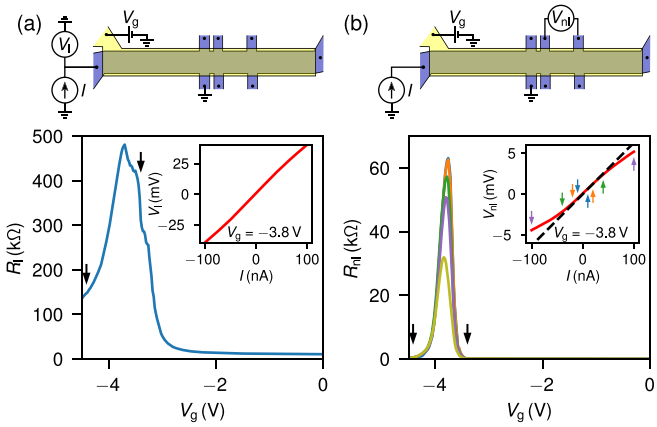


FIG. 2. Nonlocal transport measurements at $T = 4.2$ K. (a) Local two-terminal linear-response resistance of the 20-$\mu$m edge on device D1. The inset demonstrates the local $I$-$V_l$ characteristics of the edge at the CNP. (b) Nonlocal resistance measured in the configuration shown above for $I = 10$, 20, 40, 100, and 300 nA (different colors—note the blue and orange curves are almost indistinguishable). The inset demonstrates the nonlocal $I$-$V_{nl}$ characteristics.

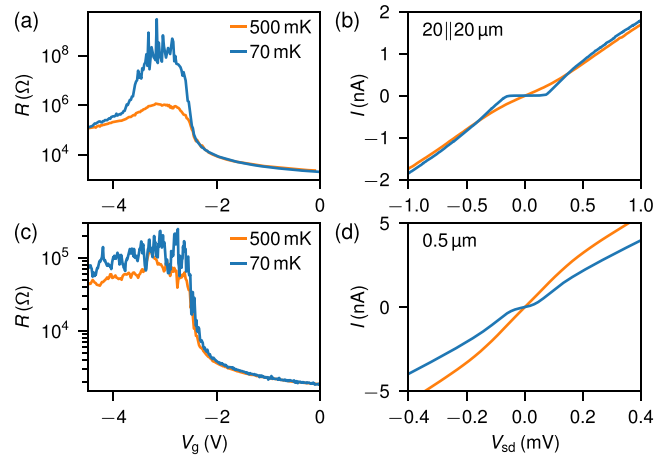


FIG. 3. Localization of the edge states at lowering the temperature on device D2. (a), (b) Two-terminal linear-response resistance as a function of $V_g$ and the $I$-$V_{sd}$ curve at the CNP for the 20-$\mu$m edge at $T = 0.5$ K (orange) and 70 mK (blue). Lowering the temperature leads to a substantial increase of resistance at the CNP accompanied by the development of significant mesoscopic fluctuations. The $I$-$V_{sd}$ curves are close to linear at $T = 0.5$ K but demonstrate a gaplike feature at $T = 70$ mK. (c), (d) Similar data for the 0.5-$\mu$m edge.

timate the bias voltages on the edges for which the bulk shunt may be safely disregarded as we now demonstrate for the 20-$\mu$m edge. Figure 2(b) demonstrates the nonlocal resistance $R_{nl} = V_{nl}/I$ measured in the configuration shown above for five different bias currents $I = 10$, 20, 40, 100, and 300 nA. In terms of $V_g$, the peak of the nonlocal signal coincides with the peak in the two-terminal resistance, and the nonzero nonlocal voltage allows one to identify the experimentally relevant range of $V_g$ (see the black arrows). For $I \lesssim 40$ nA, $R_{nl}$ is current independent which is manifested in the linear $I$-$V_{nl}$ curve [see the inset of Fig. 2(b)]. At further increasing $I$, $R_{nl}$ monotonously falls [see the green, violet, and olive curves in Fig. 2(b)] and the $I$-$V_{nl}$ curve starts demonstrating a sublinear shape, indicating the opening current leak to the ground through the bulk of the device. For the 20-$\mu$m edge, $I = 40$ nA corresponds to $V_l \approx 15$ mV which is comparable to the expected value of the bulk gap $\Delta_{bulk} \approx 30$ meV and allows one to exclude the contribution of the bulk transport at smaller biases.

We continue our discussion with the temperature dependence of the linear-response resistance $R = (dV_{sd}/dI)|_{V_{sd}<20\,\mu V}$, obtained by numerical differentiation of the $I$-$V_{sd}$ curves, of the helical edge states at sub-Kelvin temperatures in zero magnetic field on the device D2. Hereinafter, we label the straight edges of the device D2 using their length and label the several hundred nm corner-shaped edge as the "corner" [see Fig. 1(a) for the details]. For the 20-$\mu$m edge [see Fig. 3(a)], both at $V_g > -2.4$ V and at $V_g < -3.6$ V lowering the temperature from $T_1 = 0.5$ K down to $T_2 = 70$ mK only weakly influences the value of resistance reflecting the metallic-type conduction of the two-dimensional electron and hole gases. Conduction through the edge, however, demonstrates strong dielectric behavior with emerging giant mesoscopic fluctuations. Here, the increase of resistance at lowering the temperature is greater than two orders of magnitude. Assuming activationlike behavior, one can estimate the value for the activation energy for the 20-$\mu$m edge as $\Delta(20\ \mu m) \approx k_B T_2 \ln(R_2/R_1) \approx 30\ \mu$eV. Quantitatively, the discussed effect is most prominent for the long edges but it persists even for the shortest ones [see Fig. 3(c) for the case of the 0.5-$\mu$m edge]. Supplemental Material Fig. S2 [33] provides more $R(V_g)$ curves for the other edges.

The $I$-$V_{sd}$ characteristics in zero magnetic field at lowest $T$ become strongly nonlinear with the thresholdlike behavior. Figure 3(b) compares the $I$-$V_{sd}$ characteristics measured at two temperatures at the CNP for the 20-$\mu$m edge. While at 0.5 K the curve is almost linear, at 70 mK it demonstrates a gaplike feature with a threshold value of $V_{th} \approx 200\ \mu$V. We note that the corresponding energy scale is by far smaller than the bulk energy gap $\Delta_{bulk}$ of the 8-nm HgTe QWs. We also note that $eV_{th}$ is considerably greater than the estimate for the activation energy $\Delta(20\ \mu m)$. This indicates that the applied bias is shared among several strongly localized electronic states along the edge [18]. For the shorter, 0.5-$\mu$m edge, the $I$-$V_{sd}$ characteristics are qualitatively analogous, however, with a less pronounced gaplike feature and a smaller energy scale [see Fig. 3(d)]. Altogether, the observations of Fig. 3 demonstrate the localization of the edge states at lowering the temperature.

Figure 4(a) provides $R(V_g)$ curves for the 5-$\mu$m edge where we study the temperature dependence of the edge transport in details. Figure 4(b) demonstrates the $T$ dependence of the typical linear response conductance, $G_{typ} = \exp(\overline{\ln G})$, averaged in the 0.4 and 0.1 V ranges of $V_g$ in the CNP region. The estimate for the activation energy $\Delta(5\ \mu m) \approx 15\ \mu$eV is independent of the exact range of $V_g$ where the averaging is performed.

This observation of localization of the helical edge states in a 2D TI in zero magnetic field is in glaring contrast with the sub-Kelvin measurements of Refs. [18,30] where down to the

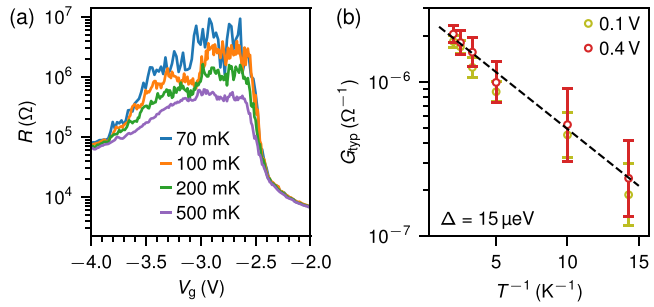


FIG. 4. Temperature dependence of the edge transport in the 5-$\mu$m edge. (a) Examples of $R(V_g)$ curves for four different temperatures. (b) Temperature dependence of the typical conductance in the CNP region averaged in the (−3 V, −2.9 V) and (−3.1 V, −2.7 V) ranges of $V_g$. The black dashed line represents activationlike behavior with a $\Delta = 15$ $\mu$eV exponent. The error bars show the standard deviation of ln $G$.

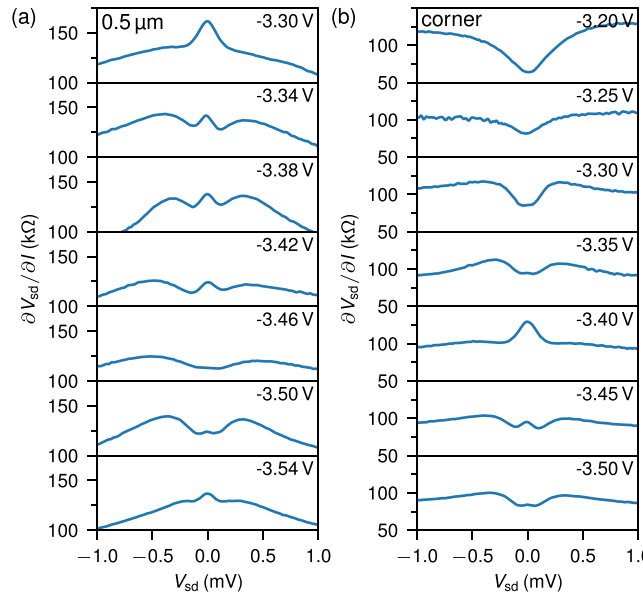


FIG. 5. Differential resistance of two short edges obtained at $B = 0$ in the CNP region at 0.5 K for (a) 0.5 $\mu$m and (b) corner edges of device D2. For various $V_g$ in the CNP region the differential resistance does not demonstrate systematic behavior as a function of bias voltage

millikelvin temperatures the edges almost did not demonstrate any $T$ dependence of conductance. We pay attention to the difference in fabrication of the devices for the case of the HgTe QWs. Here, for mesa formation we used e-beam lithography followed by wet etching, while the authors of Ref. [18] used dry Ar plasma etching applied to a photolithographically defined pattern. Yet another difference is in the way the ohmic contacts are realized—here, we evaporate Ti/Al contacts after a preliminary cap removal with the Ar gun, while in Ref. [18] the contacts were indium soldered. That being said, we are not sure the localization observed here is necessarily due to the difference in fabrication. We also note the possible correlation between the sub-Kelvin temperature behavior of the edge resistance and its value per unit length at higher temperatures. In the present paper, at 4.2 K, the edge coherence length $l_\varphi \approx L(G_q^{-1}/R)$ is close to 0.25 $\mu$m [see Supplemental Material Fig. S2(a) [33]]. Similar values were observed in Ref. [17] with an accompanying twofold resistance increase upon lowering the temperature from 4.2 K down to 0.5 K with no signs of saturation. On the contrary, relatively large values of $l_\varphi \approx 10$ $\mu$m observed at 0.8 K in Ref. [18] were obviously accompanied by far weaker or even metallic $T$ dependencies.

We now discuss the potential scenarios of localization of the helical edge states in the absence of magnetic field. The first scenario could have relied on the presence of anisotropic magnetic disorder [13,22,37]. For the case of spin $S = 1/2$ impurities, one can crudely estimate the number of impurities that would account for the conductance decrease on the order of $e^2/h$, as $N_{\text{imp}} \sim 4\xi^4 M^2/J^2 \approx 5000$, where $J \approx 0.1$ eV nm$^2$ is the anisotropic exchange coupling, $|M| = 30$ meV is the band gap, and $\xi \approx 10$ nm is the characteristic width of the edge states [37]. For the 8 nm × 10 nm × 1 $\mu$m edge with $10^6$ atoms and resistance of 100 kΩ, this number of impurities seems improbable given the QW is grown from 99.9999% pure material. This estimate indicates that magnetic impurities on their own do not dominate the edge resistance and are hardly the reason for localization. We note, however, that for the case of strong enough electron-electron interactions in the edge even a single magnetic impurity can lead to insulating behavior [38].

The nuclear spins are also known to suppress the conductance of the 2D TI edges at low temperatures provided electron-electron interactions are strong [24]. Our QWs are grown from the naturally abundant Hg and Te atoms, approximately 19% of which have a nonzero nuclear spin. In this case, the localization temperature may indeed fall in the millikelvin range, however the localization length is expected to be as high as several millimeters [39]. Thus, the hyperfine interaction is also unlikely to be the reason for localization in our micrometer long edges.

Yet another possibility for the observations of Fig. 3 is the interaction-driven localization of the disordered edges [5,6,10,40]. In this picture, the exact value of the Luttinger parameter $K$ determines not only if the localization occurs in $B = 0$ but it also defines the magnetotransport behavior. In particular, the typical edge conductance in the magnetic field $B$ is expected to obey $G_{\text{typ}} \propto \exp(-l/l_B)$, where the field-dependent localization length follows the power law $l_B \propto B^{-2/(3-2K)}$. In addition, $K$ may define the temperature and DC bias scaling of differential conductance in case the internal tunneling processes take place [11]. In our case, the edges do not demonstrate any systematic behavior with $V_{sd}$ (see Fig. 5 with the data in the vicinity of the CNP for two edges).

We perform magnetotransport measurements at $T = 0.5$ K to see if the data fit this prediction. On the one hand, this temperature is high enough so that the above discussed low-$T$ localization is not yet developed. On the other hand, we checked that at a higher temperature 4.2 K the edges generally display a relatively weak response to the external magnetic field at least up to 1.5 T [see Supplemental Material Fig. S3 [33] (note the linear scale)]. We emphasize that at 0.5 K the magnetoresistance does not demonstrate any specific features

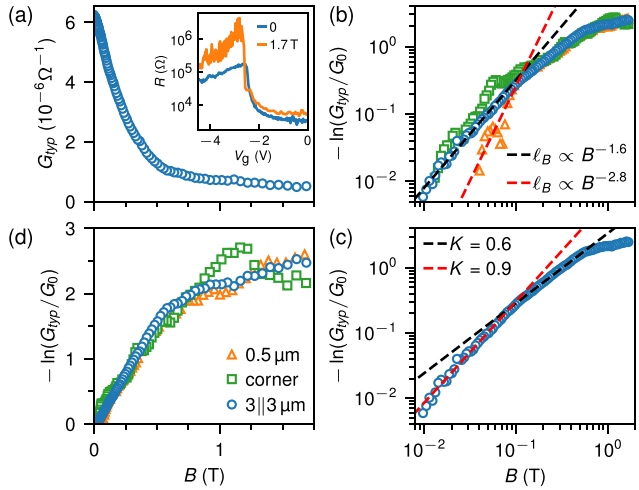


FIG. 6. Influence of the external magnetic field on the edge conductance at $T = 0.5$ K. (a) Typical conductance of the 3||3 $\mu$m edge measured in the 20 mV range of the $V_g$, as a function of the external magnetic field $B$. The inset demonstrates $R(V_g)$ curves at $B = 0$ and 1.7 T. (b) Log-log plot of the logarithm of $G_{typ}$ normalized over $G_0$ vs the magnetic field for the three edges. (c) Luttinger liquid parameter fits for the 3||3 $\mu$m edge. (d) Same as in (b) but in the linear scale.

around the critical field of aluminum which is close to 20 mT. This allows us to exclude the possible influence of superconducting contacts on our observations. Moreover, qualitatively similar behavior is observed for the edges with different distance to Al contacts (see Supplemental Material Fig. S4 [33]). Below we concentrate on the relatively short edges (see Supplemental Material Fig. S5 [33] for the results concerning the longer 20-$\mu$m edge of device D2 and the 32-$\mu$m edge of the two-terminal device D3 processed similarly to D1 and D2). The values of $K \approx 0.3$–$0.4$ observed for long edges may be a result of the finite-size effect since the Luttinger parameters extracted from the experiments characterize the interaction strength of the low-energy theory, which has a dependence on the system size. The qualitative explanation of this expectation is based on the form of renormalization group flow which for the Giamarchi-Schulz model yields a negative $dK/dL$ (see Chap. 9 in Ref. [41]).

At 0.5 K, the introduction of the magnetic field results in a substantial edge conductance decrease and development of strong mesoscopic fluctuations [see Fig. 6(a)]. Here, the $I$-$V_{sd}$ characteristics are highly nonlinear (see Supplemental Material Fig. S6 [33]). In line with Ref. [18], such behavior indicates the loss of topological protection under externally broken TRS. For the measurements of $G_{typ}$ we focus on a narrow, 20 mV, range of gate voltages in the CNP region so that the fluctuations are well reproducible in multiple $V_g$ sweeps (see Supplemental Material Fig. S7 [33]). Generally, we observe two ranges of magnetic field with two different exponents for the dependence $l_B(B)$ [see Fig. 6(b)]. At low fields $B \lesssim 0.1$ T, the localization length $l_B \propto B^{-\alpha}$, with $\alpha$ ranging approximately from 1.6 to 2.8. Despite this clear difference in the slope for different edges, the corresponding $K = 3/2 - 1/\alpha$ [10] lies in the range between 0.9 and 1.1 [see Fig. 6(c) with the data for the 3||3 $\mu$m edge]. This observation corresponds to the noninteracting disordered edge which should not localize with nonmagnetic disorder in the TRS case in contradiction with the observations of Fig. 3. At higher fields up to ≈0.5 T the dependence $l_B(B)$ slows down, with $\alpha \approx 1.1$ corresponding to $K \approx 0.6$. Note that at relatively high fields the data follow the same slope for different edges (see also Supplemental Material Fig. S8 [33] for additional data). The obtained value of $K \approx 0.6$ seemingly corresponds to a stronger interelectron interaction which may reflect the renormalization of $K$ with localization getting stronger. Still, $K \approx 0.6$ is not sufficient enough to explain localization in the absence of magnetic field according to theoretical expectations for the disordered interacting edges [5,6,10].

We note that our observations of $\alpha \sim 2$ at the relatively weak fields may be qualitatively expected also in the scenario of an edge coupled to random magnetic fluxes through the Fabry-Pérot-type loops on the boundary of a 2D TI [42]. Here, the inverse localization length $l_B^{-1} \propto \ln[G_{typ}(B)/G_0]$ shows a quadratic $B$ dependence at low $B$ followed by rapid growth and saturation when the magnetic flux through the average-area loop reaches $\approx 0.1\Phi_0 = 0.1h/e$ (see Fig. 4 of Ref. [42]). In our experiment, $B_{sat} \approx 1$ T [see Fig. 6(d)] corresponds to an average loop area of 20 nm × 20 nm. While this estimate seems reasonable for the explanation of the $B$-driven localization, it does not explain the observed localization in the absence of an external magnetic field.

## IV. CONCLUSION

In summary, we observed the localization of the helical edge states in an 8-nm HgTe quantum well in zero magnetic field at millikelvin temperatures. This result possibly heralds the importance of many-body effects in the field of topological insulators, where in terms of experiment, interaction effects are poorly studied. The observed localization is unlikely to be due to the magnetic disorder and the hyperfine interaction. While the most reasonable explanation is an interaction-driven localization of the dirty edges, the analysis of the magnetotransport data suggests that the strength of the interelectron interaction is insufficient to account for the observed localization. Our results also demonstrate that the standard transport measurements may be insufficient to unambiguously conclude on the localization mechanism, calling upon additional approaches such as, e.g., shot-noise studies [17,43] or scanning probe techniques [12,27].

## ACKNOWLEDGMENTS

This work was financially supported by the Russian Science Foundation Grant No. 18-72-10135 [44] (device fabrication, all the measurements, analysis of the magnetotransport behavior of the short edges). Fabrication of the devices was performed using the equipment of MIPT Shared Facilities Center. Influence of the external magnetic field on the conductance of the long edges was analyzed under the state task of the ISSP RAS. We thank I. S. Burmistrov, Y.-Z. Chou, V. S. Khrapai, R. M. Nandkishore, and L. Radzihovsky for useful discussions. We also thank E. M. Baeva, A. K. Grebenko, G. N. Goltsman, A. I. Kardakova, and V. N. Zverev for technical assistance.

[1] M. Z. Hasan and C. L. Kane, *Colloquium*: Topological insulators, Rev. Mod. Phys. **82**, 3045 (2010).

[2] X.-L. Qi and S.-C. Zhang, Topological insulators and superconductors, Rev. Mod. Phys. **83**, 1057 (2011).

[3] G. M. Gusev, Z. D. Kvon, E. B. Olshanetsky, A. D. Levin, Y. Krupko, J. C. Portal, N. N. Mikhailov, and S. A. Dvoretsky, Temperature dependence of the resistance of a two-dimensional topological insulator in a HgTe quantum well, Phys. Rev. B **89**, 125305 (2014).

[4] P. P. Aseev and K. E. Nagaev, Shot noise in the edge states of two-dimensional topological insulators, Phys. Rev. B **94**, 045425 (2016).

[5] C. Wu, B. A. Bernevig, and S.-C. Zhang, Helical Liquid and the Edge of Quantum Spin Hall Systems, Phys. Rev. Lett. **96**, 106401 (2006).

[6] C. Xu and J. E. Moore, Stability of the quantum spin Hall effect: Effects of interactions, disorder, and $\mathbb{Z}_2$ topology, Phys. Rev. B **73**, 045322 (2006).

[7] J. C. Y. Teo and C. L. Kane, Critical behavior of a point contact in a quantum spin Hall insulator, Phys. Rev. B **79**, 235321 (2009).

[8] A. Ström and H. Johannesson, Tunneling Between Edge States in a Quantum Spin Hall System, Phys. Rev. Lett. **102**, 096806 (2009).

[9] G. Dolcetto, M. Sassetti, and T. L. Schmidt, Edge physics in two-dimensional topological insulators, Riv. Nuovo Cimento **39**, 113 (2016).

[10] Y.-Z. Chou, R. M. Nandkishore, and L. Radzihovsky, Gapless insulating edges of dirty interacting topological insulators, Phys. Rev. B **98**, 054205 (2018).

[11] T. Li, P. Wang, H. Fu, L. Du, K. A. Schreiber, X. Mu, X. Liu, G. Sullivan, G. A. Csáthy, X. Lin, and R.-R. Du, Observation of a Helical Luttinger Liquid in InAs/GaSb Quantum Spin Hall Edges, Phys. Rev. Lett. **115**, 136804 (2015).

[12] R. Stühler, F. Reis, T. Müller, T. Helbig, T. Schwemmer, R. Thomale, J. Schäfer, and R. Claessen, Tomonaga–Luttinger liquid in the edge channels of a quantum spin Hall insulator, Nat. Phys. **16**, 47 (2020).

[13] J. I. Väyrynen, F. Geissler, and L. I. Glazman, Magnetic moments in a helical edge can make weak correlations seem strong, Phys. Rev. B **93**, 241301(R) (2016).

[14] M. König, Spin-related transport phenomena in HgTe-based quantum well structures, Ph.D. thesis, Universität Würzburg, 2007.

[15] L. Du, I. Knez, G. Sullivan, and R.-R. Du, Robust Helical Edge Transport in Gated InAs/GaSb Bilayers, Phys. Rev. Lett. **114**, 096802 (2015).

[16] E. B. Olshanetsky, Z. D. Kvon, G. M. Gusev, A. D. Levin, O. E. Raichev, N. N. Mikhailov, and S. A. Dvoretsky, Persistence of a Two-Dimensional Topological Insulator State in Wide HgTe Quantum Wells, Phys. Rev. Lett. **114**, 126802 (2015).

[17] E. S. Tikhonov, D. V. Shovkun, V. S. Khrapai, Z. D. Kvon, N. N. Mikhailov, and S. A. Dvoretsky, Shot noise of the edge transport in the inverted band HgTe quantum wells, JETP Lett. **101**, 708 (2015).

[18] S. U. Piatrusha, E. S. Tikhonov, Z. D. Kvon, N. N. Mikhailov, S. A. Dvoretsky, and V. S. Khrapai, Topological Protection Brought to Light by the Time-Reversal Symmetry Breaking, Phys. Rev. Lett. **123**, 056801 (2019).

[19] C.-Y. Hou, E.-A. Kim, and C. Chamon, Corner Junction as a Probe of Helical Edge States, Phys. Rev. Lett. **102**, 076602 (2009).

[20] T. L. Schmidt, Current Correlations in Quantum Spin Hall Insulators, Phys. Rev. Lett. **107**, 096602 (2011).

[21] J. Strunz, J. Wiedenmann, C. Fleckenstein, L. Lunczer, W. Beugeling, V. L. Müller, P. Shekhar, N. T. Ziani, S. Shamim, J. Kleinlein, H. Buhmann, B. Trauzettel, and L. W. Molenkamp, Interacting topological edge channels, Nat. Phys. **16**, 83 (2020).

[22] B. L. Altshuler, I. L. Aleiner, and V. I. Yudson, Localization at the Edge of a 2D Topological Insulator by Kondo Impurities with Random Anisotropies, Phys. Rev. Lett. **111**, 086401 (2013).

[23] A. Ström, H. Johannesson, and G. I. Japaridze, Edge Dynamics in a Quantum Spin Hall State: Effects from Rashba Spin-Orbit Interaction, Phys. Rev. Lett. **104**, 256804 (2010).

[24] C.-H. Hsu, P. Stano, J. Klinovaja, and D. Loss, Nuclear-spin-induced localization of edge states in two-dimensional topological insulators, Phys. Rev. B **96**, 081405(R) (2017).

[25] S. Wu, V. Fatemi, Q. D. Gibson, K. Watanabe, T. Taniguchi, R. J. Cava, and P. Jarillo-Herrero, Observation of the quantum spin Hall effect up to 100 kelvin in a monolayer crystal, Science **359**, 76 (2018).

[26] M. König, S. Wiedmann, C. Brüne, A. Roth, H. Buhmann, L. W. Molenkamp, X.-L. Qi, and S.-C. Zhang, Quantum spin hall insulator state in HgTe quantum wells, Science **318**, 766 (2007).

[27] E. Y. Ma, M. R. Calvo, J. Wang, B. Lian, M. Mühlbauer, C. Brüne, Y.-T. Cui, K. Lai, W. Kundhikanjana, Y. Yang, M. Baenninger, M. König, C. Ames, H. Buhmann, P. Leubner, L. W. Molenkamp, S.-C. Zhang, D. Goldhaber-Gordon, M. A. Kelly, and Z.-X. Shen, Unexpected edge conduction in mercury telluride quantum wells under broken time-reversal symmetry, Nat. Commun. **6**, 7252 (2015).

[28] C.-A. Li, S.-B. Zhang, and S.-Q. Shen, Hidden edge Dirac point and robust quantum edge transport in InAs/GaSb quantum wells, Phys. Rev. B **97**, 045420 (2018).

[29] R. Skolasinski, D. I. Pikulin, J. Alicea, and M. Wimmer, Robust helical edge transport in quantum spin Hall quantum wells, Phys. Rev. B **98**, 201404(R) (2018).

[30] T. Li, P. Wang, G. Sullivan, X. Lin, and R.-R. Du, Low-temperature conductivity of weakly interacting quantum spin Hall edges in strained-layer InAs/GaInSb, Phys. Rev. B **96**, 241406(R) (2017).

[31] S. Dvoretsky, N. Mikhailov, Y. Sidorov, V. Shvets, S. Danilov, B. Wittman, and S. Ganichev, Growth of HgTe quantum wells for IR to THz detectors, J. Electron. Mater. **39**, 918 (2010).

[32] K. Bendias, S. Shamim, O. Herrmann, A. Budewitz, P. Shekhar, P. Leubner, J. Kleinlein, E. Bocquillon, H. Buhmann, and L. W. Molenkamp, High mobility HgTe microstructures for quantum spin Hall studies, Nano Lett. **18**, 4831 (2018).

[33] See Supplemental Material at http://link.aps.org/supplemental/10.1103/PhysRevB.104.195405 for the measurement details and additional experimental data.

[34] A. Roth, C. Brüne, H. Buhmann, L. W. Molenkamp, J. Maciejko, X.-L. Qi, and S.-C. Zhang, Nonlocal transport in the quantum spin Hall state, Science **325**, 294 (2009).

[35] G. M. Gusev, Z. D. Kvon, O. A. Shegai, N. N. Mikhailov, S. A. Dvoretsky, and J. C. Portal, Transport in disordered two-dimensional topological insulators, Phys. Rev. B **84**, 121302(R) (2011).

[36] X. Liu, T. Li, S. Yao, G. Sullivan, and R.-R. Du, Transport in InAs/GaSb quantum spin Hall insulators with high-k dielectrics as the top barrier, Appl. Phys. Lett. **114**, 212101 (2019).

[37] P. D. Kurilovich, V. D. Kurilovich, I. S. Burmistrov, and M. Goldstein, Helical edge transport in the presence of a magnetic impurity, JETP Lett. **106**, 593 (2017).

[38] J. Maciejko, C. Liu, Y. Oreg, X.-L. Qi, C. Wu, and S.-C. Zhang, Kondo Effect in the Helical Edge Liquid of the Quantum Spin Hall State, Phys. Rev. Lett. **102**, 256803 (2009).

[39] C.-H. Hsu, P. Stano, J. Klinovaja, and D. Loss, Effects of nuclear spins on the transport properties of the edge of two-dimensional topological insulators, Phys. Rev. B **97**, 125432 (2018).

[40] N. Kainaris, I. V. Gornyi, S. T. Carr, and A. D. Mirlin, Conductivity of a generic helical liquid, Phys. Rev. B **90**, 075118 (2014).

[41] T. Giamarchi, *Quantum Physics in One Dimension* (Oxford Science Publications, Oxford, UK, 2003).

[42] P. Delplace, J. Li, and M. Büttiker, Magnetic-Field-Induced Localization in 2D Topological Insulators, Phys. Rev. Lett. **109**, 246803 (2012).

[43] I. Kimchi, Y.-Z. Chou, R. M. Nandkishore, and L. Radzihovsky, Anomalous localization at the boundary of an interacting topological insulator, Phys. Rev. B **101**, 035131 (2020).

[44] https://rscf.ru/project/18-72-10135/